Not for Distribution!

Comet Dust: The View after Hale-Bopp

M.S. Hanner[a]

[a]Jet Propulsion Laboratory, California Institute of Technology, Pasadena CA, 91109, USA

Extensive observations of comet Hale-Bopp from the ground and space have considerably expanded our knowledge of cometary dust. There is a clear correlation of stronger polarization, higher albedo, more prominent infrared silicate features, and higher infrared color temperature. The composition of the silicates includes both olivine and pyroxenes, in both crystalline and glassy or amorphous form, similar to the chondritic aggregate interplanetary dust particles.

1. Introduction

The apparition of comet Hale-Bopp (C/1995 O1) was a fortunate convergence of a bright comet observable for more than two years over a wide range in heliocentric distance and improved observational capabilities, enabling detailed measurements with high spatial resolution and broad wavelength coverage. ESA's Infrared Space Observatory (ISO) was in operation throughout the apparition, significantly extending the infrared observations in time and spectral range. As a result, considerable progress has been made in elucidating the properties of cometary dust.

Comet Hale-Bopp already displayed an extensive coma when discovered in July 1995 at heliocentric distance r = 7.2 AU. It soon became evident that the activity was driven by strong CO outgassing; the observed CO production rate at r = 6.6 AU was ~ 2 x 10^{28} mol/sec (Jewitt et al. 1996; Biver et al. 1996). A strong infrared signal from warm dust was already detected at 4.9 AU (Gruen et al. 2000). The comet released a prodigious amount of dust; the dust area x albedo product near perihelion was 100 times that of comet Halley (Schleicher et al. 1997). Complex patterns of jets and other structures were evident in the coma throughout the comet's apparition. Perihelion occurred on 1 April 1997 at 0.91 AU from the Sun. The comet was well observed during June to October 1996 (4.2–2.7 AU) and from February to May 1997 (1.25–0.91 AU).

This paper will highlight some of the new results from observations of the dust coma of Hale-Bopp. In particular, spatially resolved measurements of polarization and thermal emission permit us to correlate variations in several optical properties of the dust, while mid-infrared spectra have allowed us to resolve long-standing questions about the mineralogy of the cometary silicates.

2. Polarization

2.1 Observations

Polarization carries important information about the properties of the scattering particles. The polarization $P(\theta)$ as a function of phase angle θ has been established by combining measurements from a number of comets. While the polarization from different comets is similar at small phase angles, the comets tend to divide into two classes at larger θ, having P_{max} ~15% and ~25% respectively near θ 90°–100° (Chernova et al. 1993, Levasseur-Regourd et al. 1996 and references therein). Negative polarization of order −2% is observed in comets at $\theta < 20°$; both classes of comets appear to have similar negative polarization at small θ.

Comet Hale-Bopp was observed at phase angles from 7° to 47° between June 1996 and May 1997 (Furusho et al. 1999; Ganesh et al. 1998; Hadamcik et al. 1999; Hasegawa et al. 1999; Jockers et al. 1999; Kiselev and Velichko 1999; Manset and Bastien 2000). A phase curve for the average coma at λ~ 0.65 μm is shown in Fig. 1. The polarization at all phase angles is distinctly higher than that measured for previous comets, even those in the high P_{max} class, including P/Halley. At θ >30° there is a clear trend towards higher polarization at longer wavelength; the higher the polarization, the stronger the wavelength dependence. A similar, but weaker, wavelength dependence was seen in comet P/Halley (e.g., Dollfus et al. 1988).

In single-aperture measurements, negative polarization of order −0.5% to −1% was recorded at $\theta < 20°$, similar to that in other comets at similar phase angles (Ganesh et al. 1998; Manset and Bastien 2000; Kiselev and Velichko 1999). However, spatially resolved observations revealed differences in the negative polarization branch with position in the coma, with values as low as −5% near the photometric center at $\theta = 7°$ (Hadamcik 1999), while integrated measurements over the polarization image showed little or no negative polarization at all (Hadamcik 1999; Hadamcik et al. 1999; Jones and Gehrz 2000).

Widespread use of CCD arrays to construct polarization images for Hale-Bopp has facilitated the study of polarization variations within the coma (Furusho et al. 1999; Hadamcik 1999; Hadamcik et al. 1999; Jockers et al. 1999; Jones and Gehrz 2000). Structure in the polarization images generally correlates with the structure seen in images of total intensity $I \times \rho$, where ρ is the projected distance from the photometric center. The visible jets and arcs correspond to regions of higher polarization.

There is an inner region, extending a few thousand km in diameter, with lower polarization than the surrounding coma. This circumnuclear zone is evident in both 1996 and 1997, although the morphology of the inner coma changed considerably during that time. At small phase angles, this zone exhibits negative polarization down to −5% at 0.67 μm (Hadamcik 1999). A similar circumnuclear region of lower polarization was detected in several other comets, including 1P/Halley (Dollfus and Suchail 1987), C/1990 K1 Levy (Renard et al. 1992), 47P/Ashbrook-Jackson (Renard et al. 1996) and 81P/Wild 2 (Hadamcik and Levasseur-Regourd 1999). However, C/1996 Q1 Tabur and C/1996 Hyakutake displayed higher polarization in the inner 2000 km (Kolokolova et al. 2000).

2.2. Interpretation of Polarization

Interpreting the polarization in terms of particle properties is complex. The degree of polarization and its angular dependence, $P(\theta)$, depend on particle size, shape, composition, surface roughness, and aggregation. Trends, for example with composition, may differ in different particle size regimes. Predictions based on Mie theory will be inaccurate, even misleading in the general trends, for any particle shape except a smooth sphere.

Yanamandra-Fisher and Hanner (1999) studied shape effects for particles with size parameter $X = 2\pi\ a/\lambda$ in the range 1–5. While silicate spheres with $X = 2.5$ exhibit negative polarization at all θ, other shapes show $P_{max} \sim +25\%$ and negative polarization at $\theta < \theta_c$, where θ_c ranges from 20 ° to 70°. In contrast, carbon particles with $X = 2.5$ display mainly positive polarization, $P_{max} \sim 50\%$; the phase angle of maximum polarization varies with particle shape. Mishchenko (1993) computed the phase matrix for shape distributions of dirty silicate spheroids, $X = 3.5$. As the axial ratio of the spheroids increased, the polarization at intermediate phase angles changed from negative (characteristic of spheres) to positive, leaving a negative branch at 0°–30° phase angles, similar to the cometary $P(\theta)$.

In recent years, there has been encouraging progress in understanding the polarization by irregular particles, especially aggregates. Numerical methods have allowed exploration of particle shape and aggregate structure while direct scattering measurements have contributed data on particle structures too large to be handled easily by the numerical codes. West (1991) and Zerull et al. (1993) demonstrated via computation and laboratory measurements, respectively, that the polarization of a fluffy aggregate is determined primarily by the polarization properties of the constituent grains. Calculations by Kozasa et al. (1993) confirmed that, indeed, fluffy aggregates composed of spheres much smaller than the wavelength produce Rayleigh polarization. Xing and Hanner (1997) found that aggregates of intermediate porosity (~ 60%) generated polarization intermediate between that of the constituent grains and that of a compact particle with size parameter equal to that of the aggregate. They concluded that a mixture of silicate and carbonaceous aggregates of porosity ~ 60% and constituent grains of $X \sim 2.5$ could produce a polarization phase curve similar to that of comet dust.

Recently, two groups have published results of experiments designed to measure the polarization by fluffy aggregate structures:

The PROGRA^2 experiments make use of microgravity during parabolic airplane flights to levitate particles in the path of a laser and measure $P(\theta)$ (Worms et al. 1999, 2000; Hadamcik 1999; Hadamcik et al. 2000). In the recent experiments, the particles consist of submicron grains, radius < 0.1 μm ($X \leq 1$) forming fluffy aggregates. The aggregates can agglomerate into very loose structures up to millimeter size. Although the P_{max} is generally high, because of the small grain size, mixtures of silica and carbon aggregates show promise for reproducing the cometary $P(\theta)$, including negative polarization at small phase angles.

The microwave scattering laboratory at the University of Florida permits study of cometary analogue particles by scaling both the particle dimensions and the wavelength to the microwave domain (Gustafson 2000). Measurements can be made over a range of frequencies, to determine color and polarimetric color. Gustafson and Kolokolova (1999) have presented color and polarization measurements for aggregates of silicate and

absorbing grains, $0.5 < X < 20$ and have analyzed the trends of color and polarimetric color with grain size and composition. These results have led Kolokolova et al. (2000) to interpret the change in polarization with distance from the nucleus in terms of sublimating organic refractory mantles on silicate grains.

3. Correlations in Observable Quantities

In order to disentangle the effects of particle size, composition, and structure, it is useful to look at the correlations among observable quantities. The spatially resolved observations of the dust coma of Hale-Bopp and comparisons of Hale-Bopp with other comets allow us to summarize with some confidence the trends and correlations in the scattering properties of comet particles. Table 1a compares the average observed properties in the inner coma of Hale-Bopp with similar measurements of comet P/Halley. Table 1b makes a similar comparison for the jets and spirals in Hale-Bopp in February–April 1997 versus the background coma.

There is a clear correlation of higher polarization, redder polarimetric color, higher albedo, stronger silicate feature, higher infrared color temperature, and enhanced 3–5 μm thermal emission. (Although the color of the scattered light can also be diagnostic, (e.g., Kolokolova et al. 1997, 2000), we do not have consistent color data for comparing Hale-Bopp and Halley.)

3.1 Polarization

As discussed in section 2.1, comets tend to form two groups with differing P_{max}. The comets with higher P_{max} generally exhibit a strong scattered light continuum and a conspicuous silicate feature. Hale-Bopp is consistent with this trend, displaying the highest polarization at a given phase angle and strongest silicate feature ever recorded. For grains of size comparable to the wavelength (X in the approximate range 2.5–6), polarization is higher for absorbing grains than for silicate grains and carbon grains lack the negative polarization produced by silicate grains. As X increases from 2.5 to 5, P_{max} decreases for silicate grains, but increases for carbon grains with regular, but non-spherical, shapes (Yanamandra-Fisher and Hanner 1999). Thus, increased polarization could mean more absorbing grains relative to silicate grains in the coma; however, this would contradict the correlation between higher polarization and stronger silicate emission. Only if there is a significant contribution to the scattering from particles with $X < 2$, then a decrease in particle size would produce an increase in polarization for both silicate and absorbing grains, consistent with the higher silicate feature and higher 3–5 μm flux. However, for small grains, $X \lesssim 1.5$, polarization and albedo are anti-correlated, in contrast to the comet observations.

Polarization by an aggregate particle depends on the porosity and the size of constituent grains (section 2.2).

Table 1. Correlations among Observable Properties

a. Hale-Bopp versus Halley		Possible explanations
Polarization	higher	more small grains, $X < 2$ more absorbing grains, $a \sim \lambda$
Polarimetric Color	redder	more small grains, $X < 2$ more silicate grains, $a \sim \lambda$
Albedo	higher	more small grains, $a \sim 0.2$ μm more "clean" silicates
Continuum	stronger	more small grains more "clean" silicates higher dust/gas ratio
Silicate Feature	stronger	small silicate grains, $a < 1$ μm higher silicate/carbon abundance warmer silicates
Color Temperature	higher	more small absorbing grains
3-5 μm Flux	higher	more small absorbing grains, $a < 0.5$ μm

b. Jets versus Average Coma in Hale-Bopp		
Polarization	higher	more small grains, $X < 2$ more absorbing grains, $a \sim \lambda$
Polarimetric Color	redder	more small grains, $X < 2$ more silicate grains, $a \sim \lambda$
Silicate Feature	stronger	smaller silicate grains, $a < 1$ μm higher silicate/carbon abundance warmer silicates
Color Temperature	higher	more small absorbing grains
3-5 μm Flux	higher	more small absorbing grains, $a < 0.5$ μm

3.2 Polarimetric Color

Comets generally exhibit higher polarization at longer wavelength (red polarimetric color, $P(\lambda) > 0$) and $P(\lambda)$ was redder in Hale-Bopp than in Halley. Two studies of non-spherical particles are described here. Yanamandra-Fisher and Hanner (1999) carried out calculations for compact, non-spherical shapes, $X = 1 - 5$. Gustafson and Kolokolova (1999) measured the polarization by aggregate particles with porosity approximately 50% and 90%. For small, compact grains, $X < 2$, a decrease in grain size causes a redder polarimetric color, for both absorbing and silicate materials. In the limit $X << 1$, $P(\lambda) = 0$. An increase in polarization ($P(\lambda) > 0$) was measured for porous aggregates of silicate spheres as X for the spheres decreased from 1.75 to 1.32. For $X > 2$, compact absorbing grains with constant refractive index have higher polarization at larger X, thus blue polarimetric color, while silicate grains have decreasing polarization with increasing X, thus red polarimetric color. A porous aggregate of spheroids, refractive index $1.7 - 0.2i$ and $X \sim 4$ displayed slightly red polarimetic color. Compact particles with $X >> 1$ will tend toward neutral $P(\lambda) \sim 0$. The aggregates of silicate spheres with $X \sim 20$ showed essentially neutral $P(\lambda)$.

Correlations between color and polarimetric color are discussed by Gustafson and Kolokolova (1999) and Kolokolova et al. (1997, 2000).

3.3 Albedo

The average albedo, $A(\theta)$, at a given phase angle can be determined from nearly-simultaneous measurements of thermal emission and scattered light. (Note that $A(\theta)$ is neither the single-scattering albedo, which requires integration over all phase angles, nor the geometric albedo, defined for 0° phase; Hanner et al. 1981). Using the definition from Gehrz and Ney (1992) we have

$$\frac{f(\text{vis})}{f(\text{IR})} = \frac{A(\theta)}{1-A(\theta)}$$

where f (vis) and f (IR) are the integrated apparent intensities, measured at phase angle θ, of the scattered and thermal energy distributions, respectively. Mason et al. (2000) find $0.25 < A(\theta) < 0.40$ for Hale-Bopp at $20° < \theta < 40°$, significantly higher than the typical values of $A(\theta) \sim 0.20$ in comet Halley (Gehrz and Ney 1992).

There are no reliable measurements of the albedo in the jets and spiral structures. Such measurements would require accurate co-registration of simultaneous infrared and optical images having similar spatial resolution and point spread function. Strong jet activity was observed to be associated with higher albedo and bluer color in comet Halley (Tokunaga et al. 1986; Morris and Hanner 1993).

For compact, slightly or moderately absorbing grains ($k \lesssim 0.25$), the single-scattering albedo reaches a maximum at $|m - 1|X \sim 1.5$, where $m = n - ik$ is the refractive index and X is the size parameter; at $\lambda = 0.5$ μm the maximum corresponds to grain radius ~ 0.2 μm. Consequently, decreasing the mean size of the grains in the coma from micron-sized to a few tenths of a micron would tend to increase the albedo, whereas decreasing the mean

grain size below ~ 0.2 μm would tend to lower the albedo. (Since we measure the albedo at a specific phase angle, any change in the angular scattering function would also affect the observed albedo.) Loss of absorbing mantles on small silicate grains is another means of increasing the albedo. For fully absorbing grains (k > 0.25), the albedo increases monotonically with increasing grain size, so a decrease in grain size will lower the albedo.

Trends with porosity of an aggregate particle will depend on the size and absorptivity of the constituent grains. Hage and Greenberg (1990) have shown that, for aggregates having constituent grains with size parameter $X \sim 0.2$, the albedo will decrease as the porosity increases, particularly for porosity > 75%. In their aggregate model of cometary dust, Greenberg and Hage (1990) and Li and Greenberg (1998) assume that the aggregates are composed of core-mantle interstellar grains with core radius 0.1 μm and overall radius ~ 0.14 μm; for this model the albedo will decrease as porosity increases. Only if the constituent grains would have radii > 0.2 μm and $k < 0.25$ would the albedo at $\lambda = 0.5$ μm increase with increasing aggregate porosity.

A very strong scattered light continuum, with respect to the gas emission, was observed in Hale-Bopp. The scattered light continuum was 100 times stronger than that of Halley at similar distances, while the gas production rate was ~ 20 times larger (Schleicher et al. 1997). The higher albedo of the dust in Hale-Bopp can account for only a small part of the implied factor of 5 increase in the dust/gas ratio; the total cross-section of dust must have been higher relative to the gas production as well

3.4 Silicate Feature

The 10 μm silicate emission feature was stronger (as defined by the ratio of total flux/interpolated continuum at 10 μm) in Hale-Bopp than in any previous comet; total flux/continuum ratio was ~ 3 near perihelion. To show a strong, narrow 10 μm emission feature requires silicate grains with radius, $a < 1$ μm (e.g., Hanner et al. 1987). The strength of the feature in a comet depends on its visibility above the continuum produced by featureless grains of all sizes. Therefore, a stronger silicate feature could be due to a higher cross section of small silicates, relative to other dust components, or to a higher temperature of the silicates, making their feature more visible. The effect of refractory organic mantles on the silicate emission feature depends on the refractive index of the mantle material at both optical and infrared wavelengths; higher absorption at $\lambda < 1$ μm will heat the mantled grains, increasing the visibility of the feature, whereas high opacity in the infrared will reduce the feature contrast (e.g. Greenberg and Hage 1990; Li and Greenberg 1998).

Larger aggregate particles will generate a silicate feature only if the porosity is high enough for the radiation to interact primarily with the constituent submicron silicate grains. For their assumed size distributions, Greenberg and Hage (1990) and Li and Greenberg (1998) needed a porosity > 95% to produce a sufficiently strong silicate feature.

3.5 Thermal Emission

Comets typically have mid-infrared (5–13 μm) color temperatures 5–30% higher than that of an equilibrium blackbody; the ratio T_c/T_{bb} is often called the "superheat" (e.g.,

Gehrz and Ney 1992). The high T_c can be explained by absorbing grains smaller than the infrared wavelengths. Such grains absorb sunlight at visual wavelengths more efficiently than they can radiate at $\lambda > 5$ μm; they must heat up until they achieve a balance between absorbed and emitted energy. Because the grains do not radiate as blackbodies, T_c is not necessarily the physical temperature of the grains and T_c can be wavelength-dependent. The 8–13 μm superheat observed for Hale-Bopp was about 1.38 near 1 AU (Hayward et al. 2000), compared with ~ 1.15 in P/Halley (Tokunaga et al. 1988), while the T_c at 3–5 μm (Hayward et al. 2000) and 5–8 μm (Williams et al. 1998) was ~ 1.8 times the blackbody temperature, far higher than that observed in any other comet (Gehrz and Ney 1992). The 3–5 μm thermal flux is a particularly sensitive indicator of hot sub-micron sized grains (grain radius $a < 0.5$ μm). Gehrz and Ney plotted a clear correlation between the superheat and the strength of the silicate feature in their sample of comets, and Hale-Bopp fits with their plot.

Thermal images (5–18 μm) and spatially resolved 8–13 μm spectra were acquired by Hayward et al. (2000). The thermal images show the same jets and spiral structures as optical images from the same time intervals. Either the same particles were responsible for the optical and thermal excess radiation in the jets, or the two grain populations have the same dynamical properties and thus similar spatial distributions. The 8–13 μm T_c and the 3–5 μm fluxes are higher in the jets than in the background coma. The silicate feature was consistently stronger by 10–20% in the jets and spirals. In summary, there was always a correlation between the T_c, the 3–5 μm flux, and the strength of the silicate feature, both over time and with position in the coma.

Calculations of the motions of grains ejected from discrete active areas on the nucleus, as a function of their ejection velocities and $\beta = F_{rad}/F_{grav}$ indicate that the observed spiral patterns in these images are consistent with small grains having $\beta_{max} < 1$, but not small grains with $\beta_{max} > 2$ (Hayward et al. 2000). That is, the morphology is consistent with the excess radiation in jets and spirals arising from small clean or slightly absorbing silicate grains, but not with sub-micron sized absorbing grains. For submicron silicate spheres, β_{max} is < 1 when $k < 0.1$, where $m = n - ik$ is the complex refractive index.

A value of $k = 0.1$ would cause a silicate grain with $a \gtrsim 0.5$ μm to be as warm as a carbon grain. A grain of 0.1 μm radius would be significantly warmer than a blackbody, but ~100 K cooler than a carbon grain at 1 AU; these grains probably could not produce the observed 3–5 μm flux in Hale Bopp. The temperature attained by a core/mantle particle depends on the refractive index and thickness of the mantle material (cf. Greenberg and Hage 1990, Fig. 8).

3.6 Summary

No simple explanation is consistent with all of the parameters in Table 1. An increased abundance of small, slightly dirty ($k < 0.05$) silicate grains would cause a higher albedo, stronger silicate feature, and redder polarimetric color. However, their temperature would not be high enough to produce a high 3–5 μm flux nor $T_c > T_{bb}$. Their polarization would be higher only if the size parameter $X < 1.5$. A simultaneous increase of hot submicron absorbing grains would increase the 3–5 μm flux, but would tend to decrease the albedo

Whether core/mantle particles could be hot enough to give a high 3–5 μm flux, while still causing an increase in albedo is not yet clear.

A synthesis of all these trends into a single, consistent model for the cometary dust is well beyond the scope of this paper. Indeed, such modeling is just beginning. The date, authors have considered only subsets of these parameters. Issues to be resolved include the correlation of higher albedo with higher polarization, correlation of higher albedo and silicate feature with higher 3–5 μm flux, possible effects of evaporating grain mantles, and the role of porous aggregates.

4. Silicate Mineralogy

Small silicate grains (submicron to micron size) exhibit spectral features in thermal emission at 8–13 μm and 16–33 μm. These silicate features were stronger – and more structured – in Hale-Bopp than in any previously observed comet, allowing us to infer the mineralogy of the silicate grains.

The 8–13 μm spectral region was well observed from the ground from $r > 4$ AU to 0.92 AU (Hanner et al. 1999; Wooden et al. 1999; Galdemard et al. 1999; Hayward et al. 2000; Russell et al. 1997; Davies et al. 1999). An example is displayed in Fig. 2. One sees 3 maxima at 9.2, 10.0, and 11.2 μm and minor structure at 10.5 and 11.9 μm. The sharp peak at 11.2 μm is attributed to crystalline olivine, $(Mg,Fe)_2SiO_4$, based on the good spectral match with the measured spectral emissivity of Mg–rich olivine; it was first detected in comet P/Halley (Bregman et al. 1987; Campins & Ryan 1989), and subsequently observed in several new and long-period comets (Hanner et al. 1994a,b). The 11.9 μm shoulder is also due to crystalline olivine. The broad 10 μm maximum is characteristic of amorphous olivine (Stephens & Russell 1979). Crystalline olivine has a secondary maximum at 10 μm as well.

The 9.2 μm maximum, first recognized in Hale-Bopp, is a signature of pyroxene, $(Mg,Fe)SiO_3$. Both amorphous and crystalline pyroxenes can exhibit a peak near 9.2 μm (Stephens & Russell 1979; Dorschner et al. 1995; Koike et al. 1993). Crystalline pyroxenes have considerable variety in their spectral shape (Sandford and Walker 1985) and can contribute to the 10 μm maximum, the structure near 10.5 μm, and the overall width of the observed silicate feature. Thus, the major silicate minerals appear to be present in both crystalline and glassy or amorphous form.

The full 7–45 μm spectral region was observed with the ISO SWS spectrometer at r = 2.9 AU (Crovisier et al. 2000). This spectrum shows several strong peaks that correspond to laboratory spectra of Mg–rich crystalline olivine (Koike et al 1993). Minor structure is attributed to crystalline pyroxene (Wooden et al. 1999). In contrast, airborne spectra of P/Halley at 1.3 AU (the only other 16–30 μm spectra of a comet) show only weak olivine peaks at 28.4 and 23.8 μm (Herter et al. 1987; Glaccum et al. 1987). That the silicates are Mg–rich is consistent with the elemental composition of the dust measured during the Halley spacecraft encounters (Schulze et al. 1997).

The relative abundances of the various silicate components are difficult to determine from the spectra, because the strength of an observed feature will depend on the temperature of the emitting grains (as well as on their size and shape). The temperature of

small silicate grains in a comet coma is determined by the amount of sunlight they absorb at visual wavelengths. Dorschner et al. (1995) showed that the absorptivity depends on the Mg/Fe ratio. Pure Mg–pyroxene grains have extremely low absorption at visual wavelengths and, consequently, would be quite cold. For grain radius 0.5 μm, the difference between a pure Mg–pyroxene and an olivine grain with Mg/Fe = 1 can be hundreds of degrees at 1 AU (Hanner et al. 1999). However, the dust composition data from the Halley encounters showed that the silicates were usually associated with carbonaceous material (Kissel et al. 1986). Any absorbing material adhering to silicate grains will heat them.

Spectral models to match the Hale-Bopp spectra with a mixture of silicate minerals have been presented by Brucato et al. (1999), Hanner et al. (1999), Wooden et al. (1999, 2000), and Hayward et al. (2000). Wooden et al. proposed that observed changes in spectral shape with heliocentric distance could be explained by temperature differences between more transparent (cooler) Mg–rich crystalline pyroxene and less transparent (warmer) olivine grains. In their model, the crystalline pyroxene grains produce the 9.2 μm maximum in 1997 and constitute $\sim$ 95% of the small silicate grains in the coma, in order to produce observable emission at the cold temperatures.

Hayward, Hanner & Sekanina (2000) fit their spectra with a composite silicate model plus a size distribution of absorbing grains; they fit the 9.2 μm maximum with amorphous Mg–pyroxene. The same silicate mixture matched all of the 1997 spectra of the central core, the jets, and the background coma. They concluded that, even assuming all silicate components have the same temperature, small pyroxene grains (amorphous and crystalline) must be more abundant than silicate grains of an olivine composition.

Thus, while there is not a single, unique model for the silicates in Hale-Bopp, one can say that pyroxenes (either glassy or crystalline) were more abundant than grains of olivine composition, with an abundance ratio of about 2:1 or higher. Because of its strong emissivity at resonances, olivine produces a strong peak at 11.2 μm with an abundance $< 20\%$ of the total small silicate grains.

Not all comets exhibit the strong, structured silicate emission features characteristic of comets Hale-Bopp, P/Halley, C/1990 K1 Levy, and C/1993 A1 Mueller (e.g., Hanner et al. 1994, 1996). Whether the silicate grains in other comets are simply clumped into larger, optically thick particles or whether there is a real difference in the silicate mineralogy is not known.

5. Observations at Long Wavelengths

Measurements of the thermal emission at far-infrared and submillimeter wavelengths can help us to assess the abundance of large dust particles in the coma, because the emissivity of small particles decreases as $\lambda^{-\alpha}$, $1 \leq \alpha \leq 2$, while the emissivity of large particles remains essentially constant.

The far-infrared spectral domain of Hale-Bopp was surveyed from the ISO satellite. The on-board photometer (PHOT) measured the thermal flux through filters at 7–160 μm, while the spectrometers (SWS and LWS) recorded the spectrum from 5–160 μm. To fit the slope of the spectral energy distribution with a size distribution of the form $n(a) \propto a^{-\alpha}$

requires $\alpha \leq 3.5$, as shown in Fig. 3 (Gruen et al. 2000). For an outflow velocity $v(a) \propto a^{-0.5}$, this result implies that the dust production size distribution from the nucleus has $\alpha \leq 4$ and that the mass is concentrated in large particles.

Jewitt and Matthews (1999) acquired submillimeter continuum images of Hale-Bopp in 1997. The observed submillimeter spectral index of 0.6 suggests that the emitting particles were millimeter sized. A dust production rate of 1–2 x 10^6 kg/s near 1 AU was derived, giving a dust/gas mass ratio of at least 5.

Thus, despite the obvious abundance of small grains giving rise to the silicate features and high color temperature at short infrared wavelengths, the mass of the dust emitted from the nucleus of Hale-Bopp appears to have been dominated by large particles. Li and Greenberg (1998) argue that the small grains are incorporated into large, extremely fluffy aggregates with porosity > 97%. At such high porosity, these aggregates would be optically thin in the optical and mid-infrared and would be indistinguishable from a cloud of small grains.

6. Relation to IDPs and Interstellar Dust

Small comet grains, such as those apparently dominating the observed optical and infrared radiation in Hale-Bopp, are rapidly removed from the solar system by radiation pressure (as are extremely porous aggregates of such grains). Larger cometary particles will remain in bound orbits and may be swept up by the Earth. The chondritic aggregate IDPs are of likely cometary origin because some of them have high atmospheric entry speeds (Sandford 1991). These IDPs are heterogeneous aggregates of sub-micron sized silicates and other minerals in a carbonaceous matrix. The submicron grain size, high Mg/Fe abundance ratio, mix of crystalline and glassy olivine and pyroxenes, and high carbon content have no counterpart in any other known meteoritic material. These properties are a very good match with the inferred nature of cometary dust.

There are strong indications that at least one silicate component in the chondritic aggregate IDPs is of interstellar origin. Bradley (1994) argued that the common 0.1–0.5 μm glassy silicate grains, or GEMS (Glass with Embedded Metal and Sulfides) are interstellar, because of their high radiation dosage, relict microcrystals, and similarity to observed properties of interstellar silicates. FeNi inclusions are sufficient for magnetic alignment of interstellar grains (Goodman and Whittet 1995). The 10 μm spectra of GEMS show a broad maximum that varies between 9.3 and 10.0 μm from sample to sample, as one would expect for a varying mix of glassy pyroxene and olivine (Bradley et al. 1999).

So far, no isotopic anomalies have been detected in GEMS or other silicate grains in IDPs. However, strong D/H and $^{15}N/^{14}N$ anomalies, approaching cold molecular cloud values, have been measured in the carbonaceous material in which the GEMS are embedded (Keller et al. 2000; Messenger 2000). It seems plausible that the GEMS acquired these coatings in cold interstellar clouds (e.g. Greenberg 1982).

The origin (or origins) of the crystalline silicates in comets is less clear. Heating in the coma or on the nucleus is not sufficient for annealing of glassy or amorphous grains, and the 11.2 μm peak in Hale-Bopp was just as prominent at 4.6 AU preperihelion (Crovisier et

al. 1996) as at 0.92 AU. Crystalline grains can form by direct condensation from a hot gas at T=1200–1400 K. A few enstatite whiskers, ribbons, and platelets in probable cometary IDPs have growth patterns indicating such direct condensation (Bradley et al. 1983). Grain condensation could have occurred in the hot inner solar nebula or in presolar environments. If the crystalline silicates condensed in the inner solar nebula, then their presence in comets indicates large-scale mixing of high-temperature material to the cold outer regions where the comets formed.

Spectroscopy with ISO has given us a better picture of the distribution of crystalline silicates in astronomical sources. Mg–olivine was detected in the oxygen–rich outflows of some evolved stars (Waters et al. 1996) but is absent in spectra of the diffuse interstellar medium or molecular clouds such as the Trapezium. Nor are crystalline silicates detected in the circumstellar dust around most young stellar objects. Yet, crystalline olivine peaks are present in certain late-stage Herbig Ae/Be stars. The spectrum of HD100546 is very similar to that of Hale-Bopp (Malfait et al. 1998). These systems appear to have a population of sun-grazing comets, in order to explain transient gaseous emission spectral lines (e.g., Grady et al. 1997). The 11.2 μm peak is also present in the debris disk around β Pictoris (Knacke et al. 1993). Because the dynamical lifetime of the dust is shorter than the age of β Pictoris, comets are thought to be the replenishing source of the dust.

7. Conclusions

Hale-Bopp has provided a wealth of new data for determining the physical properties of cometary dust. As with all remote observations, these have to be interpreted with the aid of models based on known scattering and emitting properties of small grains. We find a clear correlation of higher polarization, higher albedo, stronger silicate feature, higher 3–5 μm flux, and higher infrared color temperature. Much work remains to be done to synthesize all of the observed correlations into a dust model consistent also with what we know about interstellar dust and IDPs of likely cometary origin.

The origin of the crystalline cometary silicates remains puzzling. If they condensed in the inner solar nebula, then their presence in comets requires extensive mixing in the solar nebula. If they are circumstellar in origin, then one has to understand why their spectral features are not seen in interstellar dust.

Future progress will come from several directions. Continued work on the scattering by irregular and aggregate particles will allow better interpretation of the correlations outlined here. NASA's space infrared telescope, SIRTF, will extend long-wavelength spectroscopy and photometry to a number of comets. Although some very interesting results have come from analysis of a small number of likely cometary IDPs, the IDPs have not been exploited as fully as they could be to aid the interpretation of remote sensing data. For example, a survey of many chondritic porous IDPs should be conducted to quantify the relative abundance of crystalline olivine, crystalline pyroxene, and glassy silicate grains and their typical dimensions. Ultimately, we can look forward to ESA's Rosetta mission and to the return of cometary samples, beginning with NASA's STARDUST mission, now en route to encounter with comet P/Wild 2 in January 2004 (Brownlee et al. 1996).

REFERENCES

N. Biver, H. Rauer, D. Despois, R. Moreno, G. Paubert, D. Bockelee-Morvan, P. Colom, J. Crovisier, E. Gerard and L. Jorda, Nature 380, 137 (1996).

J.P. Bradley, Science 265, 925 (1994).

J.P. Bradley, D.E. Brownlee and D.R. Veblen Nature 301, 473 (1983).

J.P. Bradley, L.P. Keller, T.P. Snow, M.S. Hanner, G.J. Flynn, J.C. Gezo, S.J. Clemett, D.E. Brownlee and J.E. Bowey, Science 285, 1716 (1999).

J.D. Bregman, H. Campins, F.C. Witteborn, D.H. Wooden, D.M. Rank, L.J. Allamandola, M. Cohen and A.G.G.M. Tielens, Astron. Astrophys. 187, 616 (1987).

D.E. Brownlee et al. in *Physics, Chemistry, and Dynamics of Interplanetary Dust*, B.A.S. Gustafson and M.S. Hanner, eds., ASP Conf. Series 104, 223 (1996).

J.R. Brucato, L. Colangeli, V. Mennella, P. Palumbo and E. Bussoletti, Plan. Space Sci. 47, 773 (1999).

H. Campins and E.V. Ryan, Astrophys. J. 341, 1059 (1989).

G.P. Chernova, N. N. Kiselev and K. Jockers, Icarus 103, 144 (1993).

J. Crovisier, T.Y. Brooke, M.S. Hanner, et. al., Astron. Astrophys. 315, L385 (1996).

J. Crovisier, T.Y. Brooke, K. Leech, et al., these Proceedings (2000).

J. Crovisier, K. Leech, D. Bockelee-Morvan, T.Y. Brooke, M.S. Hanner, B. Altieri, H.U. Keller and E. Lellouch, Science 275, 1904 (1997).

J.K. Davies, T.R. Geballe, M.S. Hanner, H.A. Weaver, J. Crovisier and D. Bockelee-Morvan, Earth, Moon, Planets 78, 293 (1999).

A. Dollfus, P. Bastien, J.F. Le Borgne, A.C. Levasseur-Regourd and T. Mukai, Astron. Astrophys. 206, 348 (1988).

A. Dollfus and J.L. Suchail, Astron. Astrophys. 187, 669 (1987).

J. Dorschner, B. Begemann, T. Henning, C. Jager and H. Mutschke, Astron. Astrophys. 300, 503 (1995).

R. Furusho, B. Suzuki, N. Yamamoto, H. Kawakita, T. Sasaki, Y. Shimizu and T. Kurakami, Publ. Astron. Soc. Japan 51, 367 (1999).

P. Galdemard, P.O. Lagage, D. Dubreuil, R. Jouan and P. Masse, Earth, Moon, Planets 78, 271 (1999).

S. Ganesh, U.C. Joshi, K.S. Baliyan and M.R. Deshpande, Astron. Astrophys. Suppl. Ser. 129, 489 (1998).

R.D. Gehrz and E.P. Ney, Icarus 100, 162 (1992).

W. Glaccum, S.H. Moseley, H. Campins and R.F. Lowenstein, Astron. Astrophys. 187, 635 (1987).

A.A. Goodman and D.C.B. Whittet, Astrophys. J. 455, L181, (1995).

C.A. Grady, M.L. Sitko, K.S. Bjorkman, M.R. Perez, D.K. Lynch, R.W. Russell, and M.S. Hanner, Astrophys. J. 483, 449 (1997).

J.M. Greenberg, in *Comets*, L.L. Wilkening, ed. Univ. Arizona Press, 131 (1982).

J.M. Greenberg and J.I. Hage, Astrophys. J. 361, 260 (1990).

E. Gruen, M.S. Hanner, S.B. Peschke, et al., Astron. Astrophys., submitted (2000).

B.A.S. Gustafson, in *Light Scattering by Nonspherical Particles*, M.I. Mishchenko, J. W. Hovenier and L. D. Travis, eds., Academic Press, 367 (2000).

B.A.S. Gustafson and L. Kolokolova, J. Geophys. Res. 104, 31711 (1999).

E. Hadamcik, Ph.D. dissertation, University of Paris 6 (1999).

E. Hadamcik and A.C. Levasseur-Regourd, C.R. Acad. Sci. Paris 2B C2-316 (1999).

E. Hadamcik, A.C. Levasseur-Regourd and J.B. Renard, Earth, Moon, Planets, 78, 365 (1999).

E. Hadamcik, J.B. Renard, A.C. Levasseur-Regourdand J.C. Worms, presented at IAU colloquium 181, Canterbury U.K., 10-14 April (2000).

J.I. Hage and J.M. Greenberg, Astrophys. J. 361, 251 (1990).

M.S. Hanner, R.D. Gehrz, D.E. Harker, T.L. Hayward, D.K. Lynch, C.G. Mason, R.W. Russell, D.M. Williams, D.H. Wooden and C.E. Woodward, Earth, Moon, Planets 79, 247 (1999).

M.S. Hanner, R.H. Giese, K. Weiss, and R. Zerull, Astron. Astrophys. 104, 42 (1981).

M.S. Hanner, J.A. Hackwell, R.W. Russell and D.K. Lynch, Icarus 112, 490 (1994b).

M.S. Hanner, D.K. Lynch and R.W. Russell, Astrophys. J. 425, 274 (1994a).

M.S. Hanner, D.K. Lynch, R.W. Russell, J.A. Hackwell and R. Kellogg, Icarus 124, 344 (1996).

M.S. Hanner, A.T. Tokunaga, W.F. Golisch, D.M. Griep and C.D. Kaminski, Astron. Astrophys. 187, 653 (1987).

H. Hasegawa, T. Ichikawa, S. Abe, S. Hamamura, K. Ohnishi and J. Watanabe, Earth, Moon, Planets 78, 353 (1999).

T.L. Hayward, M.S. Hanner and Z. Sekanina, Astrophys. J. 538, 428 (2000).

T. Herter, H. Campins and G.E. Gull, Astron. Astrophys. 187, 629 (1987).

D. Jewitt and H. Matthews, Astron. J. 117, 1056 (1999).

D. Jewitt, M. Senay and H. Matthews, Science 271, 1110 (1996).

K. Jockers, V.K. Rosenbush, T. Bonev and T. Credner, Earth, Moon, Planets 78, 373 (1999).

T.J. Jones and R.D. Gehrz, Icarus 143, 338 (2000).

L.P. Keller, S. Messenger and J.P. Bradley, Jour. Geophys. Res. 105, 10397 (2000).

N.N. Kiselev and F.P. Velichko, Earth, Moon, Planets 78, 347 (1999).

R.F. Knacke, S.B. Farjado-Acosta, C.M. Telesco, J.A. Hackwell, D.K. Lynch and R.W. Russell, Astrophys. J. 418, 440 (1993).

C. Koike, H. Shibai and A. Tuchiyama, Mon. Not. Roy. Astron. Soc. 264, 654 (1993).

L. Kolokolova, B.A.S. Gustafson and K. Jockers, presented at IAU Colloquium 181, Canterbury U.K., 10-14 April (2000).

L. Kolokolova, K. Jockers and G. Chernova, Icarus 126, 351 (1997).

L. Kolokolova, K. Jockers, B.A.S. Gustafson, and G. Lichtenberg, J. Geophys. Res., submitted (2000).

T. Kozasa, J. Blum, H. Okamoto and T. Mukai, Astron. Astrophys. 276, 278 (1993)

A.C. Levasseur-Regourd, E. Hadamcik and J.B. Renard, Astron. Astrophys. 313, 327 (1996).

A. Li and J.M. Greenberg, Astrophys. J. 498, L83 (1998).

K. Malfait, C. Waelkens, L.B.F.M. Waters, B. Vandenbussche, E. Huygen and M.S. de Graauw, Astron. Astrophys. 332, L25 (1998).

N. Manset and P. Bastien, Icarus 145, 203 (2000).

C.G. Mason, R.D. Gehrz, T.J. Jones, M.S. Hanner, D.M. Williams and C.E. Woodward, Astrophys. J., submitted (2000).

S. Messenger, Nature 404, 968 (2000).

M.I. Mishchenko, Appl. Opt. 32, 4652 (1993).

C.S. Morris and M.S. Hanner, Astron. J. 105, 1537 (1993).

J.B. Renard, E. Hadamcik and A.C. Levasseur-Regourd, Astron. Astrophys. 316, 263 (1996).

J.B. Renard, A.C. Levasseur-Regourd and A. Dollfus, Ann. Geophys. 10, 288 (1992).

R.W. Russell, D.K. Lynch, A.L. Mazuk, G.S. Rossano, M.S. Hanner and M.L. Sitko, Bull. Amer. Astron. Soc. 29, 1041 (1997).

S.A. Sandford, in *Origin and Evolution of Interplanetary Dust* A.C. Levasseur-Regourd and H. Hasegawa, (eds.), Kluwer Academic Publ., 397 (1991).

S.A. Sandford and R.M. Walker, Astrophys. J. 291, 838 (1985).

D.G. Schleicher, S.M. Lederer, R.L. Millis and T.L. Farnham, Science 275, 1913 (1997).

J.R. Stephens and R.W. Russell, Astrophys. J. 228, 780 (1979).

A.T. Tokunaga, W.F. Golisch, D.M. Griep, C.D. Kaminski and M.S. Hanner, Astron. J. 92, 1183 (1986).

A.T. Tokunaga, W.F. Golisch, D.M. Griep, C.D. Kaminski and M.S. Hanner, Astron. J. 96, 1971 (1988).

L.B.F.M. Waters, F.J. Molster, T. de Jong, et al., Astron. Astrophys. 315, L361 (1996).

R.A. West, Appl. Optics 30, 5316 (1991).

D.M. Williams, C.G. Mason, R.D. Gehrz, T.J. Jones, C.E. Woodward, D.E. Harker, M.S. Hanner, D.H. Wooden, F.C. Witteborn, and H.M. Butner, Astrophys. J. 489, L91 (1997).

D.H. Wooden, H.M. Butner, D.E. Harker and C.E. Woodward, C.E., Icarus 143, 126 (2000)

D.H. Wooden, D.E. Harker, C.E. Woodward, H.M. Butner, C. Koike, F.C. Witteborn and C.W. McMurtry, Astrophys. J. 517, 1034 (1999).

J.C. Worms, J.B. Renard, E. Hadamcik, A.C. Levasseur-Regourd and J.F. Gayet, Icarus 142, 281 (1999).

J.C. Worms, J.B. Renard, E. Hadamcik, A.C. Levasseur-Regourd and N. Brun-Huret, presented at IAU Colloquium 181, Canterbury U.K. 10-14 April (2000).

Z. Xing and M.S. Hanner, Astron. Astrophys. 324, 805 (1997).

P. A. Yanamandra-Fisher and M.S. Hanner, Icarus 138, 107 (1999).

R.H. Zerull, B.A.S. Gustafson, K. Schultz and E. Thiele-Corbach, Appl. Opt. 32, 4088 (1993).

Figure Legends

Fig. 1 Hale-Bopp polarization (red filter, $\lambda \sim 0.67$ μm). Filled circles: Hadamcik et al. 1999, Hadamcik 1999. Squares: Ganesh et al. 1998. Filled triangles: Manset and Bastien 2000, $\lambda = 0.68$ μm. Open triangles: Manset and Bastien, $\lambda = 0.76$ μm. Dashed curve: polarization for comets in high P_{max} group (Levasseur-Regourd et al. 1996).

Fig. 2. The silicate feature in Hale-Bopp (points) versus Halley (solid line), total flux/continuum. Spectral structure is marked. (Hanner et al. 1999).

Fig. 3. Comparison of ISO SWS and LWS spectra on 7 October 1996 (thick line) with dust models. Thin solid line: size distribution power law $\alpha = 3.5$; Dashed line: $\alpha = 3.7$ (Gruen et al. 2000).

Fig. 1 Hale–Bopp Polarization (red filter)

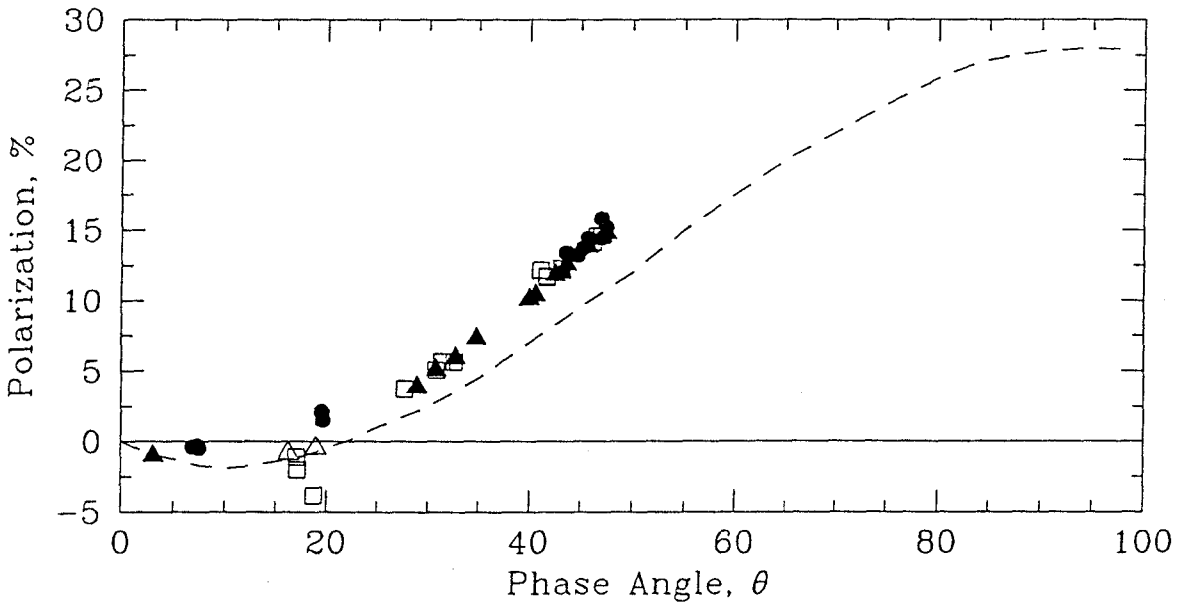

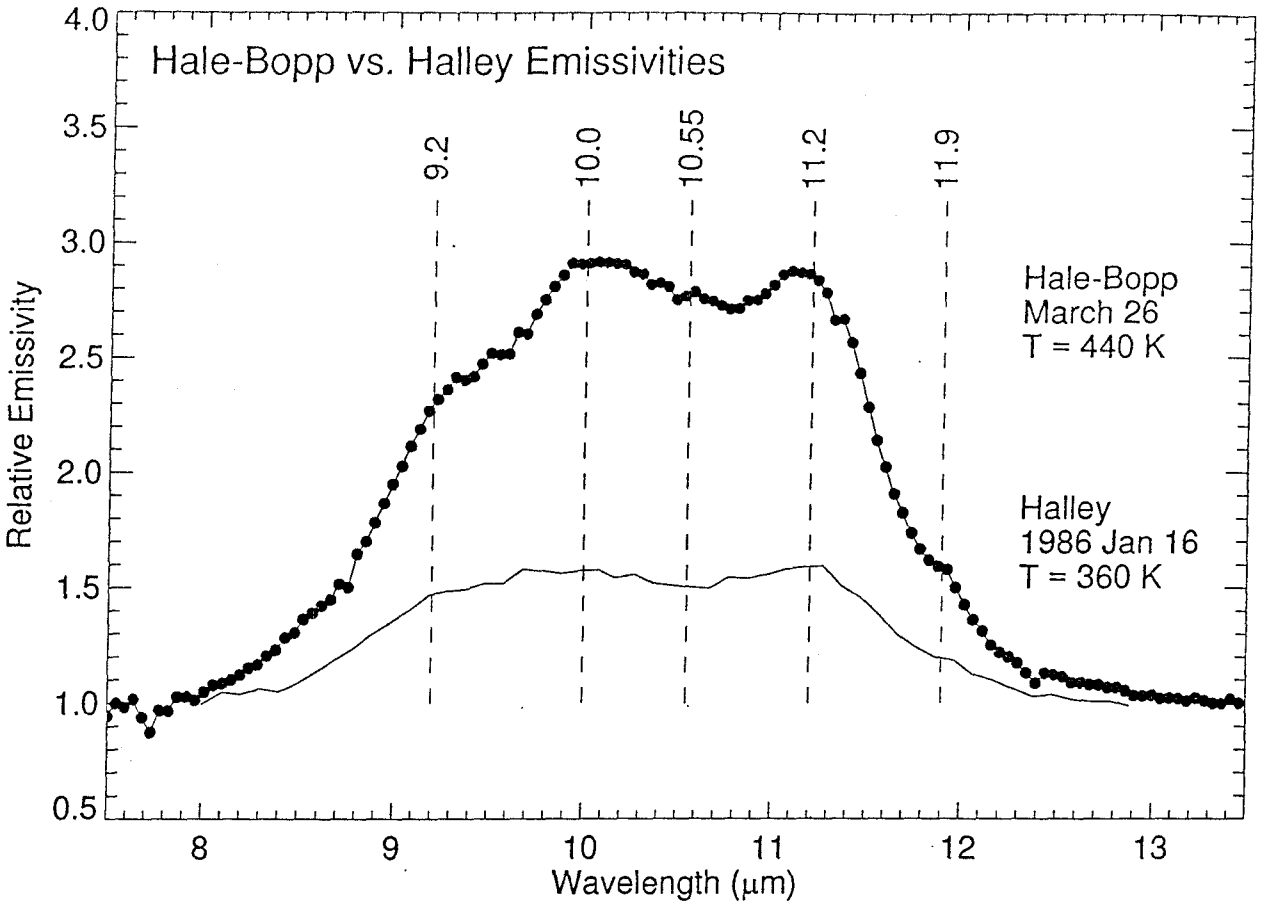
Hale-Bopp vs. Halley Emissivities
Relative Emissivity
Wavelength (μm)
9.2
10.0
10.55
11.2
11.9
Hale-Bopp
March 26
T = 440 K
Halley
1986 Jan 16
T = 360 K
4.0
3.5
3.0
2.5
2.0
1.5
1.0
0.5
8
9
10
11
12
13

Fig 2

1.5.5.